Distribution of particles suspended in convective flow in differentially heated cavity

A. L. Yarin[a)]
Faculty of Mechanical Engineering, Technion—Israel Institute of Technology, Haifa 32000, Israel

T. A. Kowalewski
Centre of Mechanics, IPPT Polish Academy of Sciences, PL 00-049, Warszawa, Poland

W. J. Hiller and St. Koch
Max-Planck-Institut für Strömungsforschung, D-37073 Göttingen, Germany

Our aim is to explore, both experimentally and theoretically, the cumulative effects of small particle–liquid density difference, where the particles are used as tracers in recirculating flow. As an example we take a flow field generated in a differentially heated cavity. The main flow structure in such a cavity consists in one or two spiraling motions. Long-term observations of such structures with the help of tracers (small particles) indicated that accumulation of the particles may set in at some flow regions. For theoretical insight into the phenomenon, a simple analytical model of recirculating (rotating) flow was studied. It was assumed that particles are spherical and rigid, and their presence does not affect the flow field. The particle Reynolds number is negligibly small, hence only the effects of particle–liquid density difference are of importance. Besides buoyancy, the effects of Saffman's force and the inertial forces are also taken into account when calculating particle trajectories. Both cases were analyzed, particles with density slightly higher and lower than the fluid. It was found that in our case the inertial forces are negligible. In the numerical experiment trajectories of particles were investigated. The particles were allocated at random in the flow field obtained by numerical solution of the natural convection in the differentially heated cavity. In the experimental part, behavior of a dilute particle suspension in the convective cell was explored. In the model-analytical study of a simple spiraling motion, it was found that due to the interaction of the recirculating convective flow field and the gravity-buoyancy force, the particles may be trapped in some flow regions, whereas the rest of the flow field becomes particle-free. This prediction agrees fairly well with the numerical and experimental findings. © *1996 American Institute of Physics.* [S1070-6631(96)01105-X]

I. INTRODUCTION

The motion of small particles settling under gravity in a fluid flow has often been investigated in the past due to its importance both in technological applications and in flow visualization. Most of the interest centered on the problem of particle mixing and sedimentation in air flow. Apart from the expected differences between particle–fluid trajectories, it was found that in some periodic cellular flows[1–6] the non-buoyant particles may remain suspended against gravity and eventually acquire asymptotic trajectories. This entrapment phenomenon has usually been interpreted in terms of inertia effects, which prevail in most practical situations.

In the present paper we deal with the case where flow velocity and particle size allow us to neglect the inertial effects completely. Also, the particles are sufficiently large for their diffusion to be neglected. The only significant forces are the buoyancy and the particle-flow viscous interaction. It is well known that even neutrally buoyant particles or droplets, on interaction with a creeping flow, may migrate across the streamlines and concentrate in some flow regions[7–10] after a sufficiently long time. Similar behavior was observed for particle tracks under natural convection in an enclosure.

Particle tracking is a very useful tool in validating a computer code simulating the flow. While the numerically generated streamlines allow detailed analysis of the flow structures, their comparison with the observed particle tracks provides the most reliable verification of the code.[11] However, due to the mass, buoyancy, and finite size of the particles, there exists an experimental uncertainty, difficult to estimate in advance. In the creeping flow regime only the buoyancy seems to be of importance. Nevertheless, good matching of particle–fluid densities is not an easy task, and in the thermal flow some disparity is always present, due to differences in their thermal expansion coefficients. These small residual effects, which may appear negligible in the short run, become important, when the long-term behavior of the tracers is studied. This is the case in our present study. The tracer particles follow periodically the cellular flow structure in the cavity, and, as we show below, the initially weak effects of their buoyancy become evident when the observation time exceeds several days.

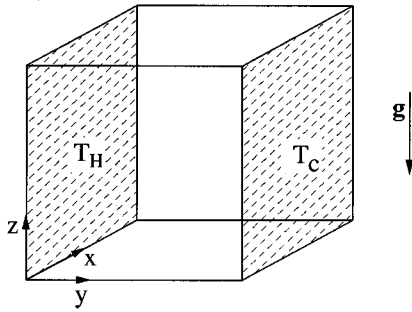[a)]Electronic mail: meralya@cnls.technion.ac.il

FIG. 1. Cubic box with two opposite, vertical isothermal walls kept at temperatures T_h (hot) and T_c (cold), respectively. The other four walls (8 mm Plexiglas) are nominally insulators. Front wall $x=0$.

The problem we deal with is three-dimensional (3-D) convection in the differentially heated enclosure (Fig. 1), often used as ''benchmark'' in verifying numerical codes. Due to the temperature gradient between the two sidewalls, the fluid inside the cavity moves. The two basic dimensionless parameters defining the problem, the Rayleigh number,

$$\text{Ra} = \frac{g \beta \, \Delta T \, L^3}{\alpha \nu}, \tag{1}$$

and the Prandtl number,

$$\text{Pr} = \frac{\nu}{\alpha}, \tag{2}$$

are used to characterize and compare the numerical and experimental results. In the above definitions, g, L, ΔT, α, β, ν denote, respectively, gravity acceleration, cavity height, the temperature difference $(T_h - T_c)$, thermal diffusivity, the coefficient of thermal expansion of the fluid and kinematic viscosity. Several visualization experiments and numerical studies[12,13] were performed in the differentially heated cube-shaped cavity. It was found that this flow has several pronounced distinctions from 2-D models. The main flow structure consists in one or two spiraling motions, responsible, besides recirculation of the liquid from the hot to the cold wall, for ''cross-flow'' from the front and back walls to the cavity center (Fig. 2). Observation of such a structure with the help of tracers has shown that accumulation of particles may be observed in some flow regions.

To get some insight of such phenomena, first we analyze the behavior of small, spherical, rigid particle in a simple model of unbounded rotating flow field. Next, we also analyze the particle behavior in a flow field generated numerically for the differentially heated cavity. The particle Reynolds number is negligibly small, hence only the effects of particle–liquid density difference are of importance. In the theoretical model, beside gravity and buoyancy, the effects of Saffman's force and the inertial forces are also taken into account when calculating particle trajectories. It is shown that even at the limit of negligible inertia and small buoyancy effects, for long observation times (days) cumulative effects of the flow–particle interaction lead to their entrapment in selected regions of the flow domain. These regions of equilibrium, located approximately midway between the front (and back) wall and the cavity center, form two closed, ring-shaped orbits, separately for heavy and buoyant par-
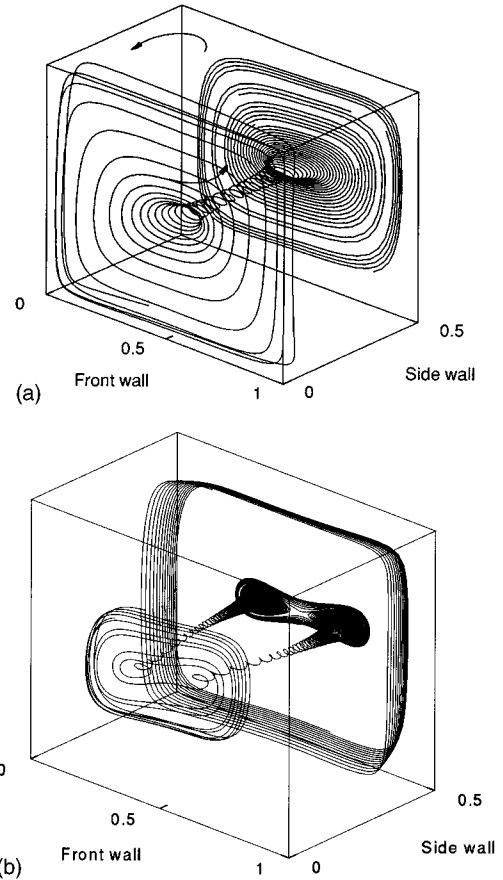

FIG. 2. Typical calculated 3-D streamlines (only front half of the cavity displayed). Pr=6300; (a) low Rayleigh number (Ra=2×10^4), inner spiral runs toward the center; (b) higher Rayleigh number (Ra=7.9×10^4), two inner spirals run toward the front wall.

ticles, whereas the rest of the cavity becomes particle-free. Our numerical and experimental observations have confirmed the existence of such regions in convective flow.

The simple model of a small rigid particle in an unbounded spiraling flow field is formulated in Sec. II. Its solution predicts accumulation of heavy and buoyant particles separately in two ring-shaped orbits. In Sec. III particle trajectories are calculated in the flow field generated as a numerical solution of the Navier–Stokes and energy equations in the differentially heated cubic enclosure. These trajectories also testify to particle accumulation in the two orbits, in both the cases where Saffman's force is neglected and taken into account. In Sec. IV experimental findings that partly confirm the theoretical predictions are presented and discussed. In Sec. V some final remarks are given. In the Appendix we discuss the effects of the neglected inertial and added mass terms for our experimental conditions.

II. FORMULATION AND SOLUTION OF A SIMPLE ANALYTICAL MODEL PROBLEM

Experimental and numerical studies[12,13] of flow in a differentially heated cubic enclosure showed at relatively low values of the Rayleigh number Ra$\lesssim 6\times10^4$ a one-roll convective cell, whereas at higher values a second roll forms (see Fig. 2). These two rolls, issuing from the ''cat's eye'' structure in the midplane, wind themselves and merge on
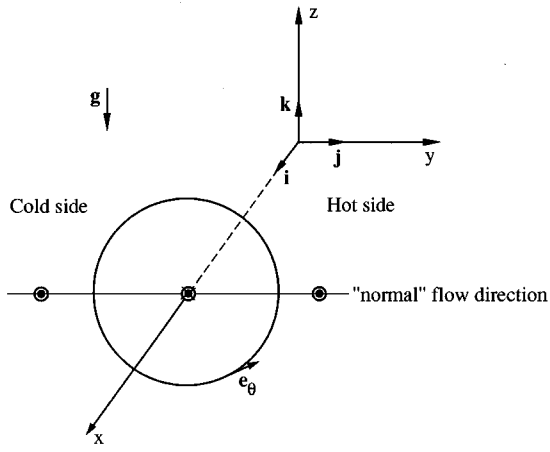
FIG. 3. Sketch of model flow. Left- and right-hand circles indicate the flow direction; in the center the flow is in the opposite direction.

their way back from the front (back) wall of the enclosure. The latter phenomenon creates an effectively one-roll configuration, except for the small, low-velocity core region. Below we show that this toroidal motion, transporting liquid back and forth along the single spiral, is a crucial factor in the effect of particle accumulation.

Let us consider a simple unbounded rotating flow field that leads itself to analytic description, while reflecting the main features of the flow in the convective cell:

$$\mathbf{v} = \omega r \mathbf{e}_\theta + V(r) \mathbf{e}_x, \tag{3}$$

where $\mathbf{v}$ is the velocity of liquid; $\mathbf{e}_\theta$ and $\mathbf{e}_x$ are the unit vectors of the azimuthal and axial directions in the cylindrical coordinate system; r is the radial coordinate; ω (=const) is the angular velocity; and $V(r)$ is the velocity component normal to the plane of rotation.

It is seen that we consider a one-roll system with an additional flow component normal to the plane of rotation (and directed toward the front or back wall of the enclosure or to its midplane). Velocity field (3) satisfies the continuity equation for an arbitrary $V(r)$. To model the basic peculiarities of the flow in the enclosure we take, for example,

$$V(r) = \begin{cases} V_0, & r < b, \\ -V_0, & r > b, \end{cases} \tag{4}$$

where V_0 is a positive or a negative constant (see Fig. 3).

Equation (4) states that there exists a core of radius b with the flow toward the front or back wall of the cell (or toward its midplane), whereas outside the core the liquid moves in the opposite direction. Both the core and outer flows transfer the liquid normally to the plane of rotation along spiraling streamlines.

Such a scheme mimics the flow structure given in Refs. 12 and 13. Reversal of the ''cross-flow'' in (4) results from its impingement on the front or back walls. The situation approximately corresponds to the flow structure for the natural convection in the cavity at relatively low Rayleigh numbers and to the effectively one-roll region of the flow at high ones.

The values of the experimental parameters used for estimations are as follows. The densities of the liquid and particles are $\rho = 1230$ kg/m^3 and $\rho_p = 1240$ kg/m^3, respectively; the length of the cubic enclosure is $L = 0.038$ m; the thermal diffusivity of liquid and Prandtl number are $\alpha = 1.01 \times 10^{-7}$ m^2/s and Pr$=1150$, respectively. The flow velocity is of the order of 100 α/L. The liquid viscosity is $\mu = 0.143$ kg/m s, whereas the radius of the particle is $a = 0.175 \times 10^{-3}$ m. Using these data, it may be shown that most of the forces acting on a particle within the flow (listed, e.g., in Refs. 2, 5, 6, and 14–16; also see the Appendix) are small compared with the Stokes and buoyancy forces. In particular, the inertia of the particle, the added mass of the liquid, the effects of pressure gradient of the flow, the augmented viscous drag from the Basset history term, the corrections for the nonuniform flow field, the Magnus and Saffman forces may be neglected. Therefore, the force balance for a particle is that of the Stokes, gravity, and buoyancy forces:

$$-6\pi\mu a(\mathbf{v}_p - \mathbf{v}) - \tfrac{4}{3}\pi a^3 (\rho_p - \rho) g \mathbf{k} = 0, \tag{5}$$

where $\mathbf{v}_p$ is the velocity of the particle, g is gravity acceleration, and $\mathbf{k}$ is the unit vector of the vertical direction (see Fig. 3).

Projection of (5) and (3) onto the Cartesian coordinate axes leads to

$$u_p = V, \tag{6a}$$

$$v_p = -\omega z_p, \tag{6b}$$

$$w_p = \omega y_p - \frac{2}{9} \frac{a^2 (\rho_p - \rho) g}{\mu}, \tag{6c}$$

where u_p, v_p, and w_p are the x, y, and z components of the particle velocity, whereas x_p, y_p, and z_p are the coordinates of the particle.

Using (6), the following set of equations describing the particle position can be written:

$$\frac{dx_p}{dt} = V, \tag{7a}$$

$$\frac{dy_p}{dt} = -\omega z_p, \tag{7b}$$

$$\frac{dz_p}{dt} = \omega y_p - \frac{2}{9} \frac{a^2 (\rho_p - \rho) g}{\mu}, \tag{7c}$$

where t denotes time.

The last two equations of (7), solved separately, yield

$$y_p = (y_{p0} - l)\cos \omega t - z_{p0} \sin \omega t + l, \tag{8a}$$

$$z_p = (y_{p0} - l)\sin \omega t + z_{p0} \cos \omega t, \tag{8b}$$

$$l = \frac{2}{9} \frac{a^2 (\rho_p - \rho) g}{\omega \mu}, \tag{8c}$$

where x_{p0}, y_{p0}, and z_{p0} are the initial positions of the particle at some moment $t = 0$.

The solution of (8) shows that the particle moves along a circle in the projection on the yz plane, with center at $y = l$, $z = 0$:

$$(y_p - l)^2 + z_p^2 = (y_{p0} - l)^2 + z_{p0}^2. \tag{9}$$

This was already encountered in geophysical applications.[17–19]

If $\rho_p > \rho$, l is positive and the center of the circle is displaced toward the ''hot'' side of the rotating flow in Fig. 3. If, by contrast, $\rho_p < \rho$, l is negative and the center is displaced toward the ''cold side.'' The symmetry is lost, since the Stokes force counteracts the gravity-buoyancy force only on one side of the cell.

Equations (8) and (9) show that in the projection on the yz plane the particle circulates with angular frequency ω, identical to that of the rotating flow. Note that the point $y = l$ and $z = 0$ corresponds to a steady-state position of the particle, since there the Stokes force is balanced by the gravity-buoyancy force.

The movement of the particle along the circle (9) takes place concurrently with its translational motion along the x axis, described by (4) and (7a), as

$$\frac{dx_p}{dt} = \begin{cases} V_0, & \sqrt{y^2 + z^2} < b, \\ -V_0, & \sqrt{y^2 + z^2} > b. \end{cases} \tag{10}$$

If part of the circle (9) is situated inside the cylinder $\sqrt{y^2 + z^2} = b$ and the remaining part is outside, then in some time intervals the particle moves with velocity V_0 (say, forward), whereas in other intervals it moves with velocity $-V_0$ (backward). Such a change of direction may result, under appropriate conditions, in the particle becoming trapped in a very short section Δx, which it is unable to leave. This means that only particles moving along such a trajectory can survive in the long term. Other particles are displaced to $x = \pm \infty$, which, in practice, means that after some delay they will settle somewhere in the cell. Therefore, some ''suspending'' trajectories should exist, where particles accumulate owing to the trapping effects, whereas other regions of the flow field are particle-free.

To find the suspending trajectory let us calculate the sojourn time of a particle inside and outside the cylinder $\sqrt{y^2 + z^2} = b$. From (8a) and (8b) we have

$$\{[(y_{p0} - l)\cos \omega t - z_{p0} \sin \omega t + l]^2 + [(y_{p0} - l)\sin \omega t + z_{p0} \cos \omega t]^2\}^{1/2} = b. \tag{11}$$

The two successive moments t_1 and t_2, when the particle crosses the cylinder, are found from (11) and given by

$$t_1 = \frac{1}{\omega}(\arccos D_1 - \arccos D_2), \tag{12a}$$

$$t_2 = \frac{1}{\omega}(2\pi - \arccos D_1 - \arccos D_2), \tag{12b}$$

where

$$D_1 = \frac{b^2 - (y_{p0} - l)^2 - z_{p0}^2 - l^2}{2l\sqrt{(y_{p0} - l)^2 + z_{p0}^2}}, \tag{13a}$$

$$D_2 = \frac{y_{p0} - l}{\sqrt{(y_{p0} - l)^2 + z_{p0}^2}}. \tag{13b}$$

Finally, the sojourn times of the particle inside the cylinder and outside it are, respectively,

$$\tau_1 = t_2 - t_1 = \frac{2\pi - 2 \arccos D_1}{\omega} \tag{14a}$$

and

$$\tau_2 = \frac{2\pi}{\omega} - \tau_1. \tag{14b}$$

The particle will remain suspended in some restricted interval of the x axis if and only if

$$\tau_1 = \tau_2, \tag{15}$$

which yields

$$\arccos D_1 = \frac{\pi}{2}, \tag{16a}$$

$$D_1 = 0 \tag{16b}$$

Using (13a) and (16b) we find that only for

$$b^2 - l^2 > 0, \tag{17}$$

a particle, whose initial position projected on yz plane, belongs to a circle,

$$(y_{p0} - l)^2 + z_{p0}^2 = b^2 - l^2, \tag{18}$$

will be captured by the flow.

Bearing in mind (9) and (18), we conclude that every particle with initial coordinates satisfying the latter will be trapped and move back and forth over a very short spiral-like trajectory along the x axis. Heavy particles ($\rho_p > \rho$) will trace this trajectory on the ''hot'' side of the flow [Fig. 4(a)] and light ones ($\rho_p < \rho$)—a similar trajectory on the ''cold'' side. All other particles will be gradually swept out and settled [Fig. 4(b)].

Returning to the natural convection in the enclosure, at the high Rayleigh number (Ra=10^5) involved here the two-roll system appears in the core. In the region of the effective vortex of both rolls, fluid is conveyed from the midplane to the front (back) wall, and returns to the midplane along the external spiral. Inside this large torus, where u (the x component of the fluid velocity) changes its direction, a non-neutrally buoyant particle can be trapped by the flow. One may expect that particles with $\rho_p > \rho$ and $\rho_p < \rho$ will survive only on two cylindrical surfaces displaced symmetrically toward the hot and cold sides of the flow. (As the flow is symmetric with respect to the plane $x = 0.5$, we limit our interest from now on to the front half of the cavity.)

III. NUMERICAL EXPERIMENT

We assume that calculation of sufficiently long trajectories of individual solid particles selected in the flow field allows us to detect existence of the equilibrium points or ''orbits'' where the tracks finally end.

A numerical simulation of the problem was performed using a finite difference solution for the velocity **v** in a differentially heated cubic enclosure containing Boussinesq fluid. The basic equations governing the flow are the vorticity transport equation,
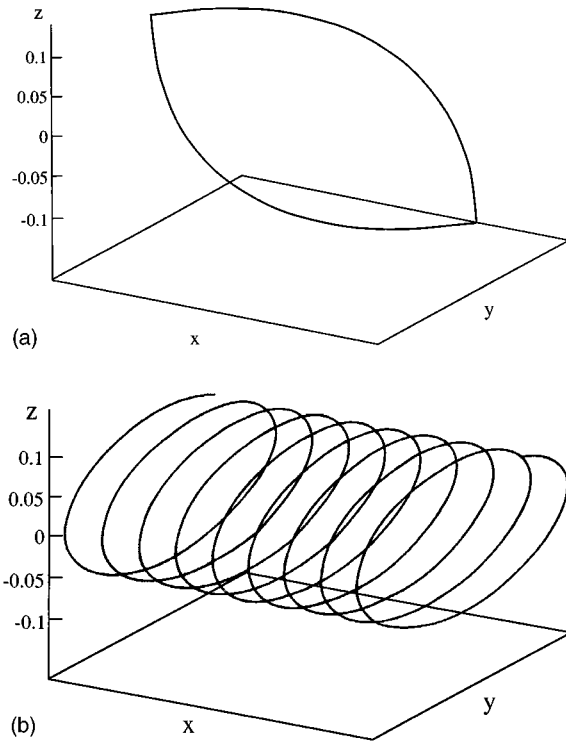
Phys. Fluids, Vol. 8, No. 5, May 1996

Yarin *et al.* 1133

FIG. 4. (a) Suspending trajectory. $x_{p0}=0$, $y_{p0}=0.1$, $z_{p0}=0$, $V_0=1$, $b=0.0887$, $\rho=1230$ kg/m^3, and $\rho_p=1240$ kg/m^3. Dimensions x, y, z, and b are scaled with cell size. The trajectory is heavily stretched along the x axis, to bring out the details. Its overall length along the x axis is 0.0166 (compare with the scale of the z axis). (b) Nonsuspending trajectory. Here $x_{p0}=0$, $y_{p0}=0.1$, $z_{p0}=0$, $V_0=1$, $b=0.2$, $\rho=1230$ kg/m^3, $\rho_p=1240$ kg/m^3. Dimensions x, y, z, and b are scaled with cell size. The trajectory is slightly stretched along the x axis. Its overall length along the x axis is 0.2999.

$$\frac{1}{\text{Pr}}\frac{\partial \mathbf{\Omega}}{\partial t}+\frac{1}{\text{Pr}}\mathbf{\nabla}\times(\mathbf{\Omega}\times\mathbf{V})=\mathbf{\nabla}^2\mathbf{\Omega}-\text{Ra}\ \mathbf{\nabla}\times\left(\theta\ \frac{\mathbf{g}}{|\mathbf{g}|}\right),\quad (19)$$

and the energy equation:

$$\frac{\partial \theta}{\partial t}+(\mathbf{V}\cdot\mathbf{\nabla})\theta=\mathbf{\nabla}^2\theta. \quad (20)$$

The vorticity vector $\mathbf{\Omega}$ is given by

$$\mathbf{\Omega}=\mathbf{\nabla}\times\mathbf{V}. \quad (21)$$

In the equations velocity $\mathbf{V}$, time t, and temperature θ are nondimensionalized, using α/L, L^2/α, and ΔT, respectively.

The steady-state solution of the equations was obtained using the 3-D code FRECON3D.[20] It is a relatively robust, false transient solver allowing quick generation of the solutions, ideal for parametric studies like the one described. The equations were discretized using a forward difference in time and central differences in space. The resulting finite difference equations were solved using the Samarskii–Andreyev Alternating Direction Scheme. The vorticity and vector-potential formulation was used. Hence, the solenoidal velocity vector field is represented by the vector potential field $\mathbf{\Psi}$:

$$\mathbf{V}=\mathbf{\nabla}\times\mathbf{\Psi}. \quad (22)$$

Substituting $\mathbf{V}$ in terms of $\mathbf{\Psi}$ and using (22), one obtains a simple relationship between the vorticity and vector potential:

$$\mathbf{\Omega}=-\mathbf{\nabla}^2\mathbf{\Psi}. \quad (23)$$

Using the definition of the velocity (22) in the vorticity transport equation (19), one obtains its final form in terms of $(\mathbf{\Omega},\mathbf{\Psi})$. In the numerical procedure the standard conservative form was adopted for the convective terms in the vorticity transport equation in order to conserve exactly the mean vorticity. It reduces numerical instabilities and improves the accuracy of the finite difference solution.

No-slip boundary conditions for the velocity were used for all six walls. The boundary conditions assumed isothermal hot and cold walls, whereas all four remaining walls were adiabatic. The solution was computed on a $61\times61\times61$ uniform mesh for experimentally equivalent conditions, i.e., Rayleigh number Ra$=10^5$ and Prandtl number Pr$=1100$. The mesh size was chosen on the basis of several tests in which its size was increased from $31\times31\times31$ to $81\times81\times81$. It was found that for the flow conditions investigated, there was no significant change in the flow generated once the mesh size exceeds 51.

To simulate tracks of individual pointwise particles, the equations of particle motion were integrated numerically for a given discrete flow field. The Kutta–Merson method with an adaptive step size was used to integrate particle tracks. To achieve high accuracy of the particle tracking at each integration step, the local fluid flow velocity and its derivatives were found by 3-D quadratic interpolation using standard subroutine DQD3DR from the IMSL library.[21] The validity of the tracks was verified in a number of ways, including variation of the mesh size and of the time step and reversal of all velocities to enable the track to be traversed in the opposite direction. It was found that a 61^3 mesh size is a justified compromise between accuracy and computation time. The tracks obtained for neutrally buoyant particles are fully reliable and the cumulative errors of integration seem to be negligible for the time scales used.

It should be noted that the main purpose of our numerical experiment was to bring out qualitative effects, rather than quantitative simulation of the physical experiment. At present, such a simulation seems to be very difficult, if at all possible. It would necessarily involve not only the full equation of motion of finite-size particles, but also nonideal thermal boundary conditions (TBC) of the physical experiment. As was found in our previous studies,[11,13] idealization of the TBC of nonisothermal walls may lead to large discrepancies between numerical particle tracking and experimental observations. Accordingly, our main attention was focused on detection of the main features in the behavior of non-neutrally buoyant particles immersed in the model flow, avoiding the numerical artifacts that may appear on further complication of the governing equations and boundary conditions.

Motion of a particle suspended in the previously computed flow field is given by Eq. (5) and the kinematic equation,

$$\frac{d\mathbf{r}_p}{dt} = \mathbf{v}_p,$$ (24)

where $\mathbf{r}_p$ is the particle position.

When Saffman's force is taken into account, Eq. (5) is replaced by

$$-6\pi\mu a(\mathbf{v}_p - \mathbf{v}) - \frac{4}{3}\pi a^3(\rho_p - \rho)g\mathbf{k}$$

$$+\frac{4}{3}\pi a^2 \frac{\mu K}{\nu^{1/2}}\frac{\mathbf{D}\cdot(\mathbf{v}-\mathbf{v}_p)}{(\mathbf{D}:\mathbf{D})^{1/4}} = 0.$$ (25)

Here ν is the kinematic viscosity of fluid, $\mathbf{D}$ is the rate-of-strain tensor, and $K = 2.594$; the expression for Saffman's force in an arbitrary flow used in (25) is based on the equation given in Ref. 15.

Integrating numerically (5) and (24) or (24) and (25), the trajectory of the virtual particle, located in the previously computed velocity field $\mathbf{v}$, was calculated. The particle tracks generated for the neutrally buoyant particles ($\rho = \rho_p$) follow the above mentioned two-spiral flow structure, traversing the cavity back and forth. Figure 5(a) shows an example of such a trajectory, which starts from the point (0.4, 0.4, 0.4), close to the midplane of the cavity. The trajectory spirals periodically toward the front wall and returns, creating a kind of toroidal structure. The trajectories generated for the heavy particles [Figs. 5(b) and 5(c)] are evidently different. After several periods of the traversing motion their spirals shrink into some small closed volumes (''bubbles''), in which accumulation of the particles can be expected.

To simulate the distribution of the suspended matter, the paths of populations of 300–1000 particles, initially distributed at random in the cavity, were generated. Their final distribution was found by monitoring particle positions after sufficiently long intervals (e.g., 140 h). This analysis consumed typically more than 24 h CPU time on a RS6000-350 workstation. The predicted final distribution is demonstrated in Fig. 6. It is found, that part of both the heavy and buoyant particles remain suspended against gravity. They follow two periodic asymptotic trajectories located in very thin coils, halfway between the front and midplanes of the cavity. Depending on the sign of the buoyancy force, the trajectories are closer to the hot or cold wall, as predicted by the solution of the analytical model in Sec. II.

With Saffman's force [Eq. (25)] taken into account, the results of the numerical simulation appeared similar to those shown above, i.e. the heavy particles are located near the hot wall, and the buoyant ones on the opposite side [Fig. 7(a)]. However, unlike the previous case, the trajectories are not confined to a single ring, but form a toroidal structure located between planes $x = 0.2$ and $x = 0.3$. The particles trapped in this region follow asymptotic trajectories along several coaxial coils [Fig. 7(b)].

IV. EXPERIMENT AND DISCUSSION

The experimental setup consisted of the convection box, a xenon flash tube, and a color CCD camera. The box, 38 mm inner dimension, had two mutually opposite vertical walls made of metal and four walls made of 8 mm thick
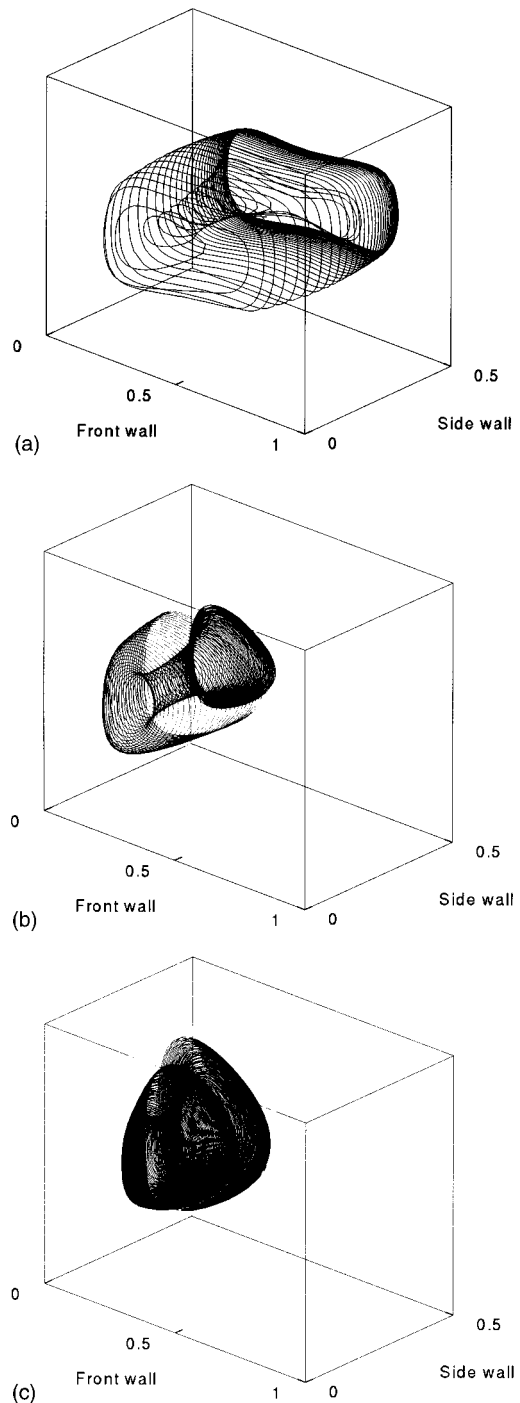

FIG. 5. Effect of buoyancy for calculated particle paths. A single particle released at point (0.4, 0.4, 0.4). Liquid density $\rho = 1230$ kg/m^3. Particle density $\rho_p = 1230$ kg/m^3 (a), 1280 kg/m^3 (b), and 1350 kg/m^3 (c), respectively. Ra$=10^5$, Pr$=1100$. Front half of the cavity displayed only. Saffman's force neglected.

plexiglas. The metal walls were kept at constant temperatures, $T_h = 25$ °C and $T_c = 20$ °C. As flow medium an aqueous solution of glycerin was used. The details of the setup have been given elsewhere.[22]

The tracer particles (irregular shape, mean size 0.35 mm) were produced from polystyrene melted with different additives with a view to the required density. Both types of par-
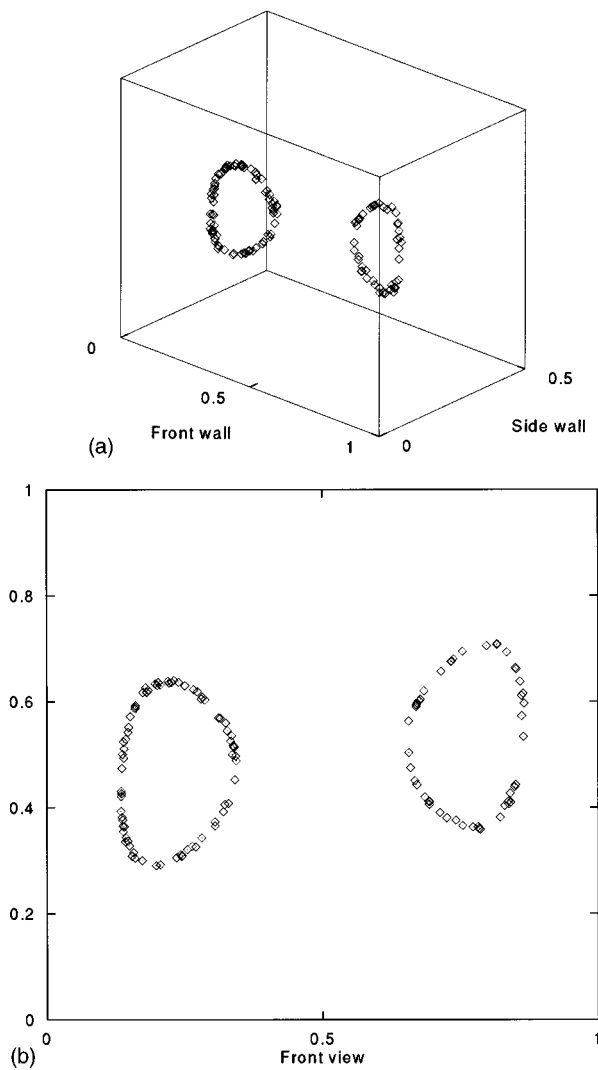
Phys. Fluids, Vol. 8, No. 5, May 1996

Yarin *et al.* 1135

FIG. 6. Calculated distribution of 300 particles, initially distributed at random, after 140 h. $Ra=10^5$, $Pr=1100$, and $\rho=1230$ kg/m^3. Only about 10% of the particles ''survived.'' Particles with 5% higher density than that of liquid $(\rho_p=1300$ kg/m$^3)$ form the ring at the hot side, those with 5% lower density $(\rho_p=1160$ kg/m$^3)$—at the cold side. Both rings located about halfway between the front and the midplane. Isometric view of the front half of the cavity (a) and front view (b). Saffman's force is neglected.

FIG. 7. Calculated distribution of 300 particles, initially distributed at random, after 140 h with Saffman's force accounted for. Here $Ra=10^5$, $Pr=1100$, and $\rho=1230$ kg/m^3. The particles with 5% higher density than that of the liquid $(\rho_p=1300$ kg/m$^3)$ form the ring at the hot side, those with 5% lower density $(\rho_p=1160$ kg/m$^3)$—at the cold side. Isometric view of the particles (a) and some of their final paths (b).

ticles, of higher and lower density (identifiable by color), were present in the flow.

The computer controlling the experiment captured periodically images of the vertical cross section of the cavity, illuminated through the 2 mm thick sheet of the flash tube. The sheet reciprocated stepwise between the front and back walls, driven by a step motor, and the images taken were evaluated to identify particles and find their positions in the image plane. A set of about 20 images yielded a full 3-D distribution of the particles in the cavity. The experiments were run uninterrupted over several days, and the collected data were successively analyzed and recorded on a hard disk. Figures 8–10 illustrate the observed development of the particle distribution.

At the time of writing, the theoretical predictions were only partly confirmed by the experimental results. Already after about 100 h (Fig. 8), we can identify an inner particle
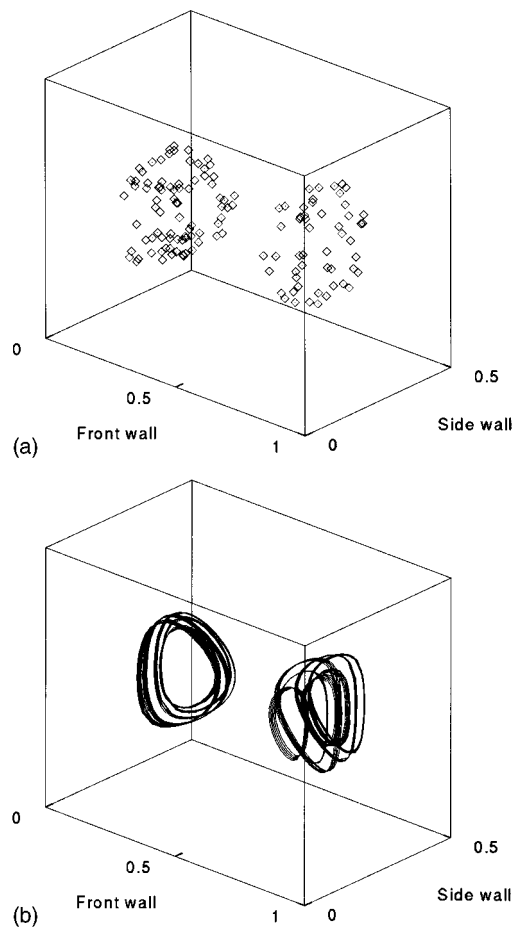
ring structure similar to the predicted one, but a second outer ring emerges. It seems that in addition to gravity, buoyancy, and Saffman's force, particle–wall interaction should also be included in the numerical model. This interaction is probably responsible for the fact that observed particles ''survive'' on the outer ring, whereas in the numerical simulation they end up at the bottom. After two weeks, almost all particles that ''survived'' form a large (3–5 mm) aggregation (Fig. 10), slowly following the circular path located near the hot wall, close to the predicted position of the left ring (cf. Fig. 6).

The experiment did not confirm the predicted accumulation of particles with density slightly lower than that of fluid in the symmetric ring on the cold side of the cavity (cf. Fig. 6). It was observed that such particles hit relatively quickly (after 20–30 h) the upper wall of the cavity and remain there permanently. This behavior is attributable to the temperature-dependent viscosity of the fluid (glycerin–water mixture). The upper regions of the cavity are warmer, hence the relative effects of buoyancy become stronger there, allowing particles to reach the upper wall before they turn back to the core of the flow.

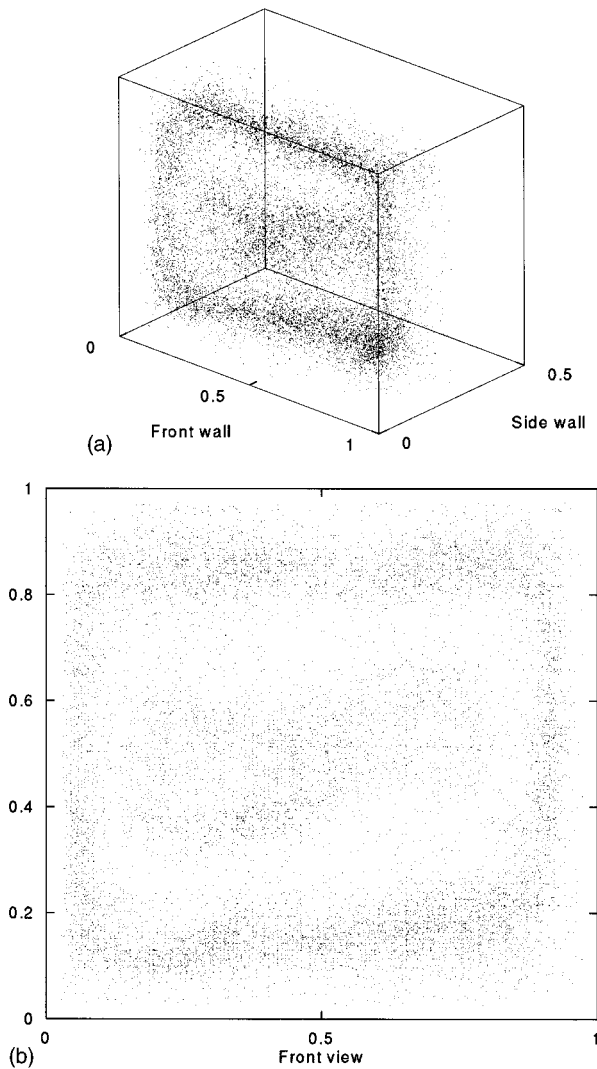On the other hand, the experiment confirmed the pre-

FIG. 8. Distribution of particles after 100 h. Here Ra=10^5, Pr=1100. Density of particles 5% higher than that of liquid. Isometric view of the front half of the cavity (a), front view (b).

FIG. 9. Multiexposed image of ''heavy'' particles after ten days (front view). Aggregation of particles observed at the left (hot) side of the plane $x=0.3$. Due to the relatively high initial particle concentration they combined together, creating a large recirculating aggregate.

enough to exclude the diffusion mechanism. Indeed, the diffusion coefficient ($D=kT/\pi\mu a$, where k is the Boltzmann constant, and T temperature) under our experimental conditions was $D=0.53\times10^{-16}$ m^2/s, which for a two-week long experiment ($t_*=1.2096\times10^6$ s) yields the diffusion drift $(Dt_*)^{1/2}=0.8\times10^{-5}$ m, which is negligibly small compared to the flow scale in the present case.

Some additional causes of particle sedimentation in the experiment of Ref. 23 may be suggested. In the present work we have seen that the flow structure in the third direction (normal to the rotation plane yz) is of crucial importance for particle retention. It may be that in the case of evaporation-driven Bénard convection of Ref. 23, the flow structure in the third direction was unsuitable for trapping. (Note that no information on the flow in the third direction is given in Ref. 23, whereas the results of Ref. 24 show that it may be com-

dicted accumulation of the heavy particles that are confined, after a sufficiently long interval, to a small region close to the hot wall. This effect is mainly due to the difference between particle and fluid density, combined with the recirculative structure of the flow. This effect may have important implications in practice. For example, in open water reservoirs, where natural convection is always present, demixing of impurities or organic species may play a crucial role in the natural cleaning processes. However, for very small particles another mechanism must be also taken into account, namely particle diffusion. This effect is discussed in Ref. 23, where particle behavior in the convective flow due to evaporation of a thin liquid layer was studied. It was found that due to the diffusion, particles suspended in the flow escaped from the convection rolls and settled on the bottom. Unfortunately, the settling particles in that study had no well-controlled diameter, so that it is impossible to determine the rate of diffusion drift there, except for the assumption that the particles were sufficiently small for diffusion to manifest itself. By contrast, the particles used in the present work were large
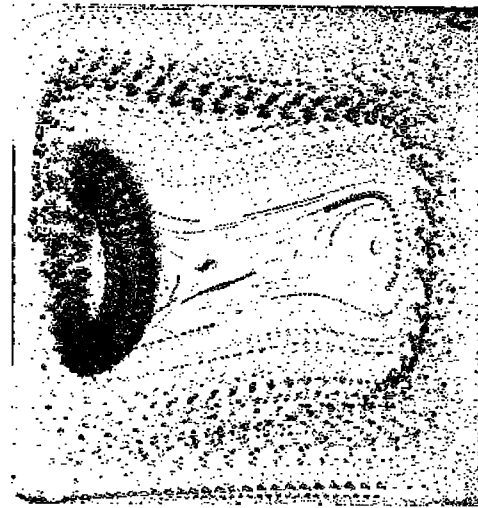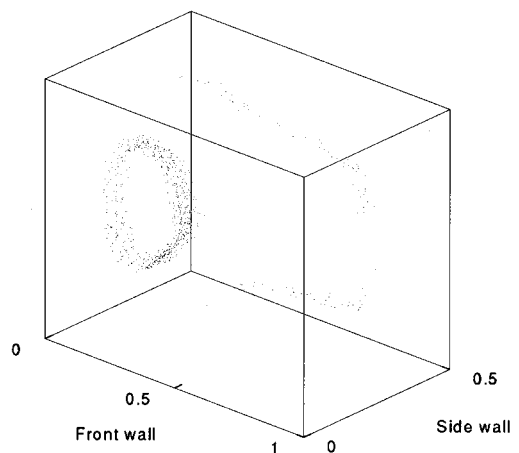

FIG. 10. Distribution of ''heavy'' particles after two weeks; isometric view of the front half of the cavity. Accumulation seen at the hot side of the cavity. Very few other particles are present in the box.

pletely different from ours, as per Fig. 2). Also, the characteristic flow velocity (enhancing particle retention) was an order of magnitude smaller in Ref. 23 than in the present work (about 0.333×10^{-4} m/s and $100\alpha/L = 0.266 \times 10^{-3}$ m/s, respectively), whereas the density difference was much larger. Moreover, the rotating flow of Ref. 23 took place in a thin fluid layer (3×10^{-3} m), where the diameter of the suspending circular trajectories (9) could be expected to be much larger than this dimension. With the particle size unspecified, this effect cannot be estimated either. Under our experimental conditions (especially for $L = 3.8 \times 10^{-2}$ m), it is impossible and the suspending coil-like trajectories are well inside the enclosure.

To sum up, the present experimental observations of particle retention (there being no doubt that it exists) are in disagreement with those of Ref. 23 due to the dissimilarities in experimental conditions.

Accumulation of sand particles in coastal waves was reported by Nielsen.[18] He pointed to a possible simple trapping mechanism due to interaction of the settling velocity with two-dimensional vortex flow. This result is directly related to our 3-D generalization of the problem, described in Sec. II. However, in view of the relatively large density difference and typically high flow velocities, the inertial effects, neglected completely in our case, must become crucial in the transportation of sand by water waves. These were thoroughly implemented by Tio et al.[5,6] and Raju et al.,[25] who analyzed the dynamics of particles in a periodic two-dimensional Stuart vortex flow or mixing layers, taking into account inertial terms in the equations of particle motion. In the Appendix we examined the influence of these additional terms in our case, with the conclusion that their effect is at least five orders of magnitude too small to affect the observed particle accumulation. The present finding indicates that in creeping periodic convective flow particle demixing will occur if only some particle–fluid density difference remains.

V. CONCLUSION

Particle accumulation in recirculating 3-D convective flow due to rotating flow-buoyancy interaction was predicted theoretically and observed experimentally. The mechanism of particle trapping involves the effect of the third component of flow (normal to the circulation plane), which to the best of our knowledge was not recognized before.

The observed particle accumulation in convective flow, apart from its importance in many technological applications, is also of interest for basic understanding of low Reynolds number fluid/particle interactions. The recirculating character of the flow allows long-term observation of the same set of particles. Hence, relatively simple experiments can be used to verify existing models describing ''lift'' forces imposed on a sphere interacting with a shear flow or a plane wall.

In the present simulations the contribution of Saffman's force was found to be of second order compared with the overall accumulation effects. Its main feature was slight thickening of the final ''coil'' representing the trajectories of the trapped particles.

It is emphasized that this is only a preliminary investigation, and for direct comparison with experiment additional factors (particle shape, nonideal thermal boundary conditions, and non-Boussinesq approximation for the fluid) have to be taken into account. Such effects as particle-induced changes in the flow field (not really negligible for rather large particles), particle–particle interaction when accumulation starts, and thermal expansion of the particles will modify the observed scenario. Nevertheless, even without such refinements our findings allow us to state that visualization of the flow using non-neutrally buoyant particles (what is practically always the case in a thermal flow), even for a creeping flow regime, may result in long-term problems.

APPENDIX: INERTIAL EFFECTS

Let us estimate the long-range effect of the inertial forces on a particle circulating in the yz plane given by (9). In addition to (5), we now account for the inertia of particle, the added mass of liquid and the effects of the pressure gradient in the flow. Therefore, the force balance for a particle now reads[2] as

$$\left(\rho_p + \frac{1}{2}\rho\right)\frac{4}{3}\pi a^3 \frac{d\mathbf{v}_p}{dt}$$

$$= -6\pi\mu a(\mathbf{v}_p - \mathbf{v}) - \frac{4}{3}\pi a^3(\rho_p - \rho)g\mathbf{k} + \frac{4}{3}\pi a^3$$

$$\times \rho\left(\mathbf{v}\cdot\nabla\mathbf{v} + \frac{1}{2}\mathbf{v}_p\cdot\nabla\mathbf{v}\right), \tag{A1}$$

which is supplemented by the kinematic equation (24).

In Eq. (A1), all terms related to the liquid velocity $\mathbf{v}$ are calculated at the particle position $\mathbf{r}_p$. Note also that for $\mathbf{v}$ as per (3) and (4), the corrections for nonuniformity of the flow field[2] vanish, since $\nabla^2\mathbf{v} = \mathbf{0}$.

Projecting (24) and (A1) on the yz plane, for the flow field described by (3), we can write

$$\frac{dy_p}{dt} = v_p, \tag{A2a}$$

$$\frac{dz_p}{dt} = w_p, \tag{A2b}$$

$$\left(\rho_p + \frac{1}{2}\rho\right)\frac{4}{3}\pi a^3 \frac{dv_p}{dt}$$

$$= -6\pi\mu a(v_p + \omega z_p) - \frac{4}{3}\pi a^3\rho\left(\omega^2 y_p + \frac{1}{2}\omega w_p\right) \tag{A2c}$$

$$\left(\rho_p + \frac{1}{2}\rho\right)\frac{4}{3}\pi a^3 \frac{dw_p}{dt}$$

$$= -6\pi\mu a(w_p - \omega y_p) - \frac{4}{3}\pi a^3(\rho_p - \rho)g + \frac{4}{3}\pi a^3\rho$$

$$\times\left(-\omega^2 z_p + \frac{1}{2}\omega v_p\right). \tag{A2d}$$

Eliminating y_p and z_p by differentiating (A2c) and (A2d) and substituting (A2a) and (A2b), we arrive at the following set of equations for v_p and w_p:

$$\epsilon\frac{d^2 w_p}{d\bar{t}^2} + \frac{dw_p}{d\bar{t}} + \epsilon R w_p - \frac{\epsilon R}{2}\frac{dv_p}{d\bar{t}} = v_p, \tag{A3a}$$

$$\epsilon\frac{d^2 v_p}{d\bar{t}^2} + \frac{dv_p}{d\bar{t}} + \epsilon R v_p + \frac{\epsilon R}{2}\frac{dw_p}{d\bar{t}} = -w_p, \tag{A3b}$$

where nondimensional time $\bar{t} = \omega t$, and

$$R = \frac{\rho}{\rho_p + \rho/2}, \tag{A4a}$$

$$\epsilon = \frac{2a^2(\rho_p + \rho/2)\omega}{9\mu}. \tag{A4b}$$

The rotational velocity of the flow is of the order of ωL. In our experiment this velocity is of the order of $100\alpha/L$. Thus, $\omega \simeq 100\alpha/L^2$, and using the values of the physical parameters, we obtain the estimate of our Reynolds number $\epsilon = 0.62\times10^{-6}$. The latter shows that in our case the inertial effects are very small, and can manifest themselves only after a very long delay. Indeed, solving Eqs. (A3) and retaining only the terms that do not vanish for large $\bar{t}$ and $\epsilon \ll 1$, we find

$$v_p = \exp\left[\epsilon\bar{t}\left(1 - \frac{3}{2}R\right)\right](C_2\cos\bar{t} - C_1\sin\bar{t}), \tag{A5a}$$

$$w_p = \exp\left[\epsilon\bar{t}\left(1 - \frac{3}{2}R\right)\right](C_1\cos\bar{t} + C_2\sin\bar{t}), \tag{A5b}$$

where C_1 and C_2 are constants.

Substituting (A5) in (A2c) and (A2d) and satisfying the initial conditions, we find (in the same leading-order long-term approximation) the following expressions for the particle trajectory:

$$y_p = e^{Et}[(y_{p0} - l)\cos\omega t - z_{p0}\sin\omega t] + l, \tag{A6a}$$

$$z_p = e^{Et}[(y_{p0} - l)\sin\omega t + z_{p0}\cos\omega t], \tag{A6b}$$

where l is given by (8c) and

$$E = \frac{2}{9}\frac{a^2(\rho_p + \rho/2)\omega^2}{\mu}\left(\frac{\rho_p - \rho}{\rho_p + \rho/2}\right). \tag{A7}$$

Thus, the yz projection of the trajectory is given by

$$(y_p - l)^2 + z_p^2 = e^{2Et}[(y_{p0} - l)^2 + z_{p0}^2]. \tag{A8}$$

With only particle inertia and added mass accounted for, (A7) reduces to

$$E = \frac{2}{9}\frac{a^2(\rho_p + \rho/2)\omega^2}{\mu}, \tag{A9}$$

whereas (A8) still holds.

Equations (A8) and (A9) show that the long-range motion of the particles (with particle inertia and added mass accounted for) follows spiral trajectories with exponentially growing radius. Taking into account also the effect of the pressure gradient in the unperturbed flow [Eqs. (A8) and (A7)], we find that heavy particles follow spiraling trajectories of growing radius (since for $\rho_p > \rho$, $E > 0$), whereas buoyant particles follow collapsing spirals (for $\rho_p < \rho$, $E < 0$), approaching the equilibrium point $y = l$, $z = 0$.

In reality the above-mentioned inertial effects can manifest themselves at time values of order

$$t_{ch} = \frac{1}{|E|} = \frac{9}{2}\frac{\mu}{a^2\omega^2|\rho_p - \rho|}. \tag{A10}$$

For the values of the parameters listed above, we estimate $t_{ch} = 4.29\times10^{10}$ s ≈ 1360 yr. In other words, all inertial effects are negligible under the conditions of the present experiment, and particle suspension on very short cylindrical surfaces, as predicted by (3)–(18), is valid.

[1] H. Stommel, ''Trajectories of small bodies sinking slowly through convection cells,'' J. Marine Res. **8**, 24 (1949).

[2] M. R. Maxey, ''The motion of small spherical particles in a cellular flow field,'' Phys. Fluids **30**, 1915 (1987).

[3] J. B. McLaughlin, ''Particle size effects on Lagrangian turbulence,'' Phys. Fluids **31**, 2544 (1988).

[4] L. Yu, C. Grebogi, and E. Ott, ''Fractal structure in physical space in the dispersion of particles in fluids,'' in *Nonlinear Structure in Physical Systems*, edited by L. Lam and H. C. Morris (Springer-Verlag, New York, 1990), p. 223.

[5] K.-K. Tio, A. M. Gañán-Calvo, and J. C. Lasheras, ''The dynamics of small, heavy, rigid particles in a periodic Stuart vortex flow,'' Phys. Fluids A **5**, 1679 (1993).

[6] K.-K. Tio, A. Liñán, J. C. Lasheras, and A. M. Gañán-Calvo, ''On the dynamics of buoyant and heavy particles in a periodic Stuart vortex flow,'' J. Fluid Mech. **254**, 671 (1993).

[7] G. Segre and A. Silberberg, ''Behavior of macroscopic rigid spheres in Poiseuille flow,'' J. Fluid Mech. **14**, 136 (1962).

[8] A. Karnis, H. L. Goldsmith, and S. G. Mason, ''The flow of suspensions through tubes,'' Can. J. Chem. Eng. **44**, 181 (1966).

[9] T. A. Kowalewski, ''Concentration and velocity measurements in the flow of droplet suspensions through a tube,'' Exp. Fluids **2**, 213 (1984).

[10] W. Hiller and T. A. Kowalewski, ''An experimental study of the lateral migration of a droplet in a creeping flow,'' Exp. Fluids **5**, 43 (1987).

[11] T. A. Kowalewski, W. J. Hiller, and G. de Vahl Davis, ''Computations and experimental visualization in heat and mass transfer problems,'' *Proceedings of the 1st Japanese–Polish Joint Seminar in Advanced Computer Simulation*, Tokyo 1993, edited by M. Akiyama, M. Kleiber, and P. Wolanski (University of Tokyo, Tokyo, 1994), p. 60.

[12] W. J. Hiller, St. Koch, and T. A. Kowalewski, ''Three-dimensional structures in laminar natural convection in a cubic enclosure,'' Exp. Thermal Fluid Sci. **2**, 34 (1989).

[13] W. J. Hiller, St. Koch, T. A. Kowalewski, G. de Vahl Davis, and M. Behnia, ''Experimental and numerical investigation of natural convection in a cube with two heated side walls,'' in *Proceedings of the IUTAM Symposium*, Cambridge, United Kingdom 13–18 August 1989, Topological Fluid Mechanics (Cambridge University Press, Cambridge, 1990), edited by H. K. Moffat and A. Tsinober, p. 717.

[14] M. R. Maxey and J. J. Riley, ''Equation of motion for a small rigid sphere in a nonuniform flow,'' Phys. Fluids **26**, 883 (1983).

[15] A. Li and G. Ahmadi, ''Deposition of aerosols on surfaces in a turbulent channel flow,'' Int. J. Eng. Sci. **31**, 435 (1993).

[16] R. I. Nigmatulin, *Dynamics of Multiphase Media* (Hemisphere, New York, 1991).

[17] M. J. Manton, ''On the motion of a small particle in the atmosphere,'' Boundary Layer Meteorol. **6**, 487 (1974).

[18] P. Nielsen, ''On the motion of suspended sand particles,'' J. Geophys. Res. **89**, 616 (1984).

[19] J. C. Lasheras and K.-K. Tio, ''Dynamics of a small spherical particle in a steady two-dimensional vortex flows,'' Appl. Mech. Rev. **47**, S61 (1994).

[20] L. P. Goh, E. Leonardi, and G. de Vahl-Davis, ''FRECON3D—Users Manual. A program for the numerical solution of mixed convection in 3-D rectangular cavity,'' UNSW, School of Mechanical and Industrial Engineering, Report 1988/FMT/7 (UNSW, Sydney, 1988).

[21] IMSL MATH/LIBRARY, User's Manual, p. 616, Houston, TX, 1992.

[22] W. Hiller, St. Koch, T. A. Kowalewski, and F. Stella, ''Onset of natural convection in a cube,'' Int. J. Heat Mass Transfer **36**, 3251 (1993).

[23] B. Simon and Y. Pomeau, ''Free and guided convection in evaporating layers of aqueous solutions of sucrose. Transport and sedimentation of solid particles,'' Phys. Fluids A **3**, 380 (1991).

[24] F. Stella, G. Guj, and E. Leonardi, ''The Rayleigh–Bénard problem in intermediate bounded domains,'' J. Fluid Mech. **254**, 375 (1993).

[25] N. Raju and E. Meiburg, ''The accumulation and dispersion of heavy particles in forced two-dimensional mixing layers. Part 2: The effect of gravity,'' Phys. Fluids **7**, 1241 (1995).